Engineering Science and Technology, an International Journal 47 (2023) 101555

Contents lists available at ScienceDirect

Engineering Science and Technology, an International Journal

journal homepage: www.elsevier.com/locate/jestch

Optimization of a novel drive mechanism approaching the ideal cycle for beta type Stirling engines

Erkan Öztürk [a,1]

[a] Pamukkale University, Faculty of Technology, Department of Automotive Engineering, Denizli, Turkey

ARTICLE INFO

Keywords:
Stirling engine
Ideal cycle
Hypocycloid
Drive mechanism
Piston dwell

ABSTRACT

Stirling engines are capable in the renewable energy gain and the recovery of waste heat, both of which are important issues today. Existing studies revealed that the piston trajectories convergent to the Stirling cycle provide more power than traditional crank mechanism. In this study, a hypocycloid drive mechanism not used in the literature was optimized on the ideal piston trajectories for beta type Stirling engines. Optimization was realized to improve the isochoric heating and cooling processes as well as the isothermal compression and expansion. The cyclic work was treated as another objective succession. The optimal results taking into account these five objectives were obtained with the gear ratios of 5 and 4 for displacer piston and power piston, respectively. The piston dwells provided the enough objective succession not only for the both isochoric processes but also for the isothermal compression process, while failed in the isothermal expansion. In comparison with crank mechanism, a cyclic work increment of 10% was achieved in the near-ideal piston trajectories, but the maximum increment of 14% eventuated in some out of ideal.

1. Introduction

In recent years the increases in energy usage and fluctuations in fuel prices have created the need for clean and cheap energy. In addition to environmental factors, the decrease in crude oil sources has required the orientation to renewable energy systems and the productive usage of sources [1]. Issues such as alternative and renewable energy sources and the recovery of waste heat have become the most studied subjects today [2–4].

While the use of electrical machines is increasing day by day in every field, electrical energy ranks first among the types of energy demanded [5,6]. Although renewable energy sources such as solar, geothermal, biomass and wind are suitable for meeting this demand, a large part of the world's energy consumption is still provided by fossil resources [7]. In fact, even the seven-hour period of solar radiation falling on the earth's surface is at a level to meet the annual energy consumption of the world [8]. The high cost, inefficiency and low specific power of systems suitable for the conversion of solar energy are the most important factors limiting the use of these systems [9,10].

Stirling engines, as closed cycle external heat engines, are machines suitable for energy conversion from various heat sources, such as geothermal, biomass, nuclear and fossil fuels as well as solar energy, and also to harness the waste heat energy [11,12]. Compared to internal combustion engines, Stirling engines have lower emission, noise and vibration characteristics as well as low maintenance requirements [13,14]. Although patented before most heat engines, Stirling engines did not receive as much attention as internal combustion engines due to their low specific power, low efficiency and long start-up period [15,16].

In theory, the thermal efficiency of Stirling engines is considered equal to the Carnot efficiency, which is known as the maximum efficiency that can be achieved with heat engines [17]. However, the real efficiency of Stirling engines has not yet reached the value of internal combustion engines [14]. Mechanical, heat and flow losses are important factors that affect the efficiency of the Stirling engines [18,19]. Heat transfer coefficients of the used materials, working fluid properties and regenerator efficiency are the main reasons for these losses. The drive mechanisms used in Stirling engines also directly affect these losses.

In Stirling engines having the wide variety depending on the application area, different drive mechanisms are used. The main types that also have commercial applications are the slider-crank, rhombic, free piston, splash plate, Ross yoke and scotch yoke mechanisms [20]. Although these mechanisms are not compatible with all Stirling engine configurations, they have some advantages among themselves. For example, free-piston Stirling engines have a high power-to-weight ratio

E-mail address: erkanozturk@pau.edu.tr.
[1] ORCID: 0000-0002-6142-972X.

https://doi.org/10.1016/j.jestch.2023.101555
Received 16 August 2023; Received in revised form 29 September 2023; Accepted 16 October 2023
Available online 20 October 2023

because they contain fewer components. Another example, low friction forces on the piston side surface are considered as an advantage for the rhombic mechanism. However, these mechanisms involve sinusoidal piston movements that do not approximate ideal Stirling cycle volume changes.

Kojima [21] examined the maximum work that can be achieved with ideal piston movements. In this study, the different cycles were compared, and it was determined that the Stirling cycle with isochoric heat input had a higher work capacity and efficiency than Otto cycle for the same compression ratio and volume values. Similar results have also been mentioned in Ref. [22]. Ranieri et al. [23] stated that a significant part of the low efficiency in Stirling engines is due to the sinusoidal movement of the pistons. By using a discrete isothermal model, they determined that only 66 % of the ideal cycle work and 27 % of Carnot efficiency can be achieved with sinusoidal approximations. They also concluded that these results determined for the alpha type were similar to the other configurations of Stirling engines, namely as beta and gamma. Scheunert et al. [24] examined the non-sinusoidal movements of both pistons for an alpha-type engine and stated that an increase up to 50 % in power output could be obtained. Another result of this study is that the optimum piston movements are quite close for the different regenerator effectiveness. In other studies of the same authors on alpha type engines [25,26], piston movements were optimized by assuming ideal regenerator and taking into account the effects of mechanical frictions. These studies were built on the endoreversible thermodynamic model, and the piston dwells at the top dead center (TDC) and bottom dead center (BDC) were changed. The common result of both studies is that optimum piston movements would provide an increase in power. In Ref. [26], it was also indicated that the longer resting durations of the cold and hot volumes would be more appropriate for mechanisms with low friction coefficient, while vice versa for high frictional coefficient.

Bert et al. [27] examined the effect of piston movements on gamma type Stirling engine by using the finite-time thermodynamic models validated experimentally. They have stated that the optimum kinematics is close to the slider-crank mechanism; nevertheless a power enhancement of 22 % can be achieved by using piston movements that generate the ideal pressure–volume diagram of Stirling cycle. It also has been concluded that this improvement may vary for the different fluids and operating speeds. In a study that focused on the effect of operating speed on piston movements to maximize power, it had been observed that the dwell durations of the pistons should be increased more for low speeds [28]. Torre et al. [29] examined the effect of ideal volume variations using a CFD model validated with experimental results of the beta Stirling engine. They found that the ideal volume variations can provide a significant gain in power and efficiency according to sinusoidal, if the heat exchangers are optimized for the ideal case. Another CFD model study validated by experimental data of an alpha Stirling engine was conducted by Tian et al. [30]. It has been concluded that the proper piston movements are crucial to decrease the throttling loss as well as isochoric heating and cooling processes. They additionally stated that engine performance can be nearly doubled by achieving both requirements.

The above-mentioned studies theorized only on the optimization of piston movements, which were not offered any mechanisms. Craun and Bamieh [31] suggested the active control of displacer piston for the beta Stirling engines. In this study, an effort has been carried out to increase the mechanical power by using Schmidt's isothermal approach. They achieved a higher power about 42 % with the displacer piston control and stated that this increase occurred during the non-sinusoidal motion with high harmonic content. A similar study including experimental data as well as theoretical analyses has been done by Briggs et al. [32]. The authors have performed this study on the free-piston Stirling engine and concluded that a theoretical power output increase of 58 % can be obtained with the high harmonic movements of the power and displacer pistons. However, an increase of only 14 % has been obtained experimentally due to the inability to reach the high harmonic waveform in the displacer piston of a free-piston engine. In addition the results based on the nodal analysis revealed that the optimum solution can be obtained in a waveform between the ideal and sinusoidal approaches. In a similar study on the control of the pistons with the motor/generator unit, Cullen and McGovern [33] examined theoretically the isothermal expansion and compression processes of the Stirling cycle, and emphasized the necessity of slow heat transfer for isothermal processes.

The structures mechanically linked of pistons are defined as kinematic Stirling engines. A gamma type solar Stirling engine running with low temperature difference was examined by Boutammachte and Knorr [34]. The discontinuous and sinusoidal displacer piston motions were discussed in terms of power output. Discontinuous movements were performed by using the cam mechanism. It was reported as an experimental outcome that the discontinuous displacer motion may be affect positively the engine power, but negatively the mechanical stability due to higher inertial forces. Wong and Goh [35] experimentally studied the effects on the engine performance of a gamma type Stirling engine with non-sinusoidal movements. They drove both pistons by cam profiles grooving to each side of flywheel. With different cam profiles trials, they achieved an increase up to 36 % in thermal efficiency with respect to sinusoidal piston movements. The main reasons for this increase were noted to be the longer dwell durations at dead centers and overlapping of pistons. Karabulut et al. [36] performed the thermodynamic analysis for alpha type Stirling engines with coaxial cylinders and conventional V-arrangement. They have indicated that the thermal efficiency can be increased up to 25 % owing to the heating at constant volume. Seto and Nobes [37] experimentally researched the improvement of thermodynamic performance for a gamma type Stirling engine with an elliptical gear drive mechanism. The elliptical gears that had different eccentricities were used for the different dwell duration combinations of both pistons. A result of the study was that the long dwell duration at dead centers for the power piston and vice versa for the displacer piston would be more suitable for gamma type engines. Another study including the elliptical gear drive mechanism was performed in Ref. [38] for alpha type Stirling engines. A slight improvement in thermal efficiency was determined using an adiabatic model for a mechanism providing an approximation of ideal piston movements. Kota [39] suggested a dwell mechanism instead of rhombic used in beta type Stirling engines. Although better piston movements are ensured, the increase in the number of parts in the mechanism is stated as a disadvantage.

According to Shendage et al. [40] the rhombic mechanism can produce up to 10 % more power than slider-crank without sacrificing efficiency. Furthermore, it was noted that the overlapping piston motions had a significant impact on performance. Ref. [41] discussed the effects of rhombic-drive geometrical variables on the performance. A result of this theoretical study based on isothermal model was that the optimum phase angle had an increasing effect on power and thermal efficiency due to decrease in dead volume.

The studies carried out so far have shown that ideal piston movements contribute positively to Stirling engine power and efficiency. However, the mechanisms used in the literature generally have a sinusoidal approach similar to the crank mechanism. A few studies have provided the kinematic mechanism with an ideal Stirling cycle approach. In these studies, either sufficient performance was not achieved for isochoric processes or isothermal processes were compromised, resulting in a reduction in power. The current study primarily offers a novel mechanism that provides ideal piston movements for beta type Stirling engines and not yet used in the literature. Additionally, the dimensions of the mechanism have been optimized to provide both isochoric and isothermal processes and by taking into account a higher power value than the sinusoidal approach. The positive and negative aspects of these novel hypocycloid drive mechanism are also discussed in detail as comparatively with traditional crank mechanism.

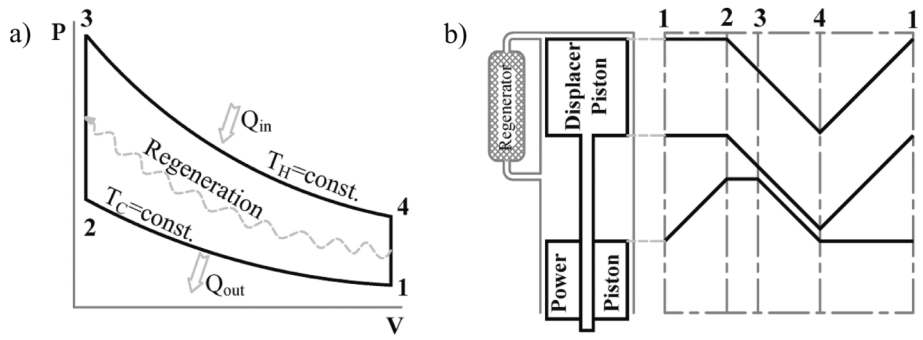

Fig. 1. a) Ideal Stirling cycle Pressure-Volume indicator diagram, b) the ideal trajectories of pistons for beta type Stirling engines [32,49].

2. Beta configuration of Stirling engines

The most important technicality that distinguishes the beta from other Stirling engine configurations is the movement of both pistons within the same cylinder. This detail enables more compact engines with the beta configuration and, thus, higher specific power between kinematic Stirling engines [42–44]. Free piston Stirling engines are also generally produced in the beta configuration, taking this fact into account [45]. However, alpha type engines are more suitable for systems with the high temperature difference between sources, while vice versa is true for gamma type engines. Low system efficiency in parallel with the low temperature difference and needing additional systems to increase the temperature difference are inevitable for solar systems, especially [46,47]. On the other hand, the beta configuration can be optimized over a wider range of temperature ratios.

The pressure–volume (PV) indicator diagram of the ideal Stirling cycle and the ideal piston trajectories of the beta configuration are given in Fig. 1. In between 1 and 2 points, isothermal compression process occurs. During this process, all working fluid must be in cold volume space and compressed by power piston. The zero mass in hot volume space is essential to maintain constant temperature and thermal equilibrium. Therefore, the displacer must remain still at TDC during this process; in other words the hot volume must be zero. The isochoric heating process (2–3) occurs inside the regenerator. Working fluid is transferred from cold volume to hot volume space via the movement of the displacer piston towards the power piston. During this process, the constant volume is achieved by the dwelling period of power piston, and the working fluid temperature reaches from the cold volume temperature (T_C) to hot volume temperature (T_H). For the isothermal expansion process (3–4), the co-movement (overlapping) of both pistons so as to provide the zero-cold volume space is an important issue. Thus, the power piston can be pushed to BDC by the heat drawn from the hot source without any heat dissipation to the cold sink. The heat removal from working fluid occurs under isochoric conditions (4–1). While the power piston dwells at BDC, the displacer piston moves towards TDC and the working fluid is transferred through the regenerator from cold volume to hot volume space. During this process, the heat on working fluid is stored in the regenerator matrix.

However, the ideal cycle does not occur adequately in real Stirling engines because of the non-isothermal conditions and insufficiencies of drive mechanisms for isochoric conditions as well as flow and heat transfer losses [23,48]. For an approximation to the ideal cycle of beta Stirling engine, the power piston dwelling periods at both dead centers and of displacer piston at only TDC are essential, as well as the movement of pistons in the same direction during the isothermal expansion process. Also, the dwell duration of power piston between 2 and 3 can be kept shorter than 4–1 owing to the increase in mass density at compressed volume that enhances the heat transfer rate.

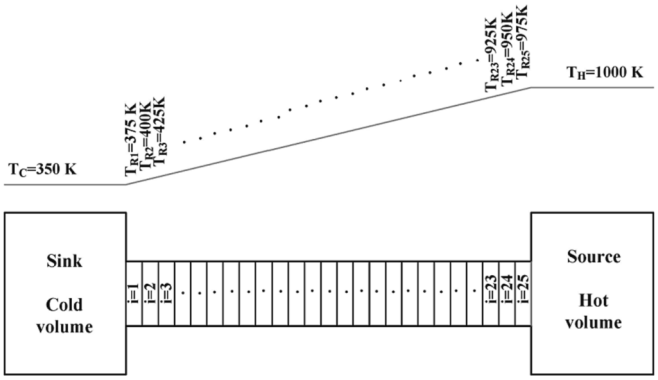

Fig. 2. Analyze wall temperatures.

3. Thermodynamic model

Thermodynamic analysis has been performed to observe changes in PV indicator diagrams and cyclic works. The isothermal approach is preferred since mechanism optimization has been performed to approach the ideal Stirling cycle. Other reasons for this preference are the shorter computation duration of isothermal analyses and the experimental factor requirements of other approaches [50–52]. Considering that the mechanisms are compared using the same parameters, the effects of the losses may be ignored.

The isothermal analysis assumes that the working fluid temperatures in the hot and cold spaces are equal to the source (TH) and sink (TC) temperatures, respectively. In addition, other assumptions are that the working fluid is air behaved as ideal gas, processes are reversible, there is no pressure difference between volumes, the fluid mass in the system is constant, and regeneration is perfect. While hot and cold volumes were regarded as monospace, the regenerator volume was divided into cells in order to provide the linear temperature distribution between hot and cold volume temperatures as seen in Fig. 2. Ensuring a temperature difference of 25 K between the adjacent cells from the sink (350 K) to the source (1000 K), 25 cells were considered sufficient [53].

The instantaneous system pressure (p) can be determined by using Eq. (1) [54]. Where, m, R, V and T are total mass of working fluid, gas constant, volume and temperature, while the subscript identifiers C, H and Ri express the cold, hot and regenerator spaces, respectively.

$$p = \frac{mR}{\frac{V_H}{T_H} + \sum_{i=1}^{25} \frac{V_{Ri}}{T_{Ri}} + \frac{V_C}{T_C}} \tag{1}$$

The diameter of both pistons was treated as equal so that they can travel in the same cylinder, especially in order to ensure overlapping at isothermal expansion process. In this way, volumes were determined from the distances between the pistons and cylinder. These distances based on the crank angle are mechanism-specific and are formulated in

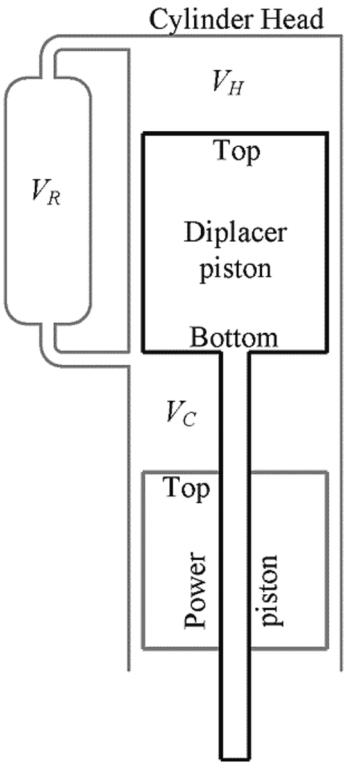

Fig. 3. System volumes.

the following section. Principally, in the isothermal analysis, thermal efficiency is equal to Carnot efficiency. Therefore, cyclic work was only considered as a performance index and determined as Eq. (2) with the integration of whole cycle intervals [17].

$$W = \oint p dV \tag{2}$$

The isothermal model used in this study is compatible with the analysis results of the beta type Stirling engine with crank mechanism in ref. [55] experimentally verified with refs. [10,56].

4. Kinematics of mechanisms

The hypocycloid drive mechanism suggested in this study was compared with the crank mechanism commonly used in Stirling engines. A similar hypocycloid drive mechanism was studied in the internal combustion engine to minimize side force between piston and cylinder [57]. However, in the present study, the hypocycloid mechanism was used to obtain harmonic piston movements. The hot and cold volumes were determined with kinematic relations for both mechanisms. As can be seen from Fig. 3, the hot volume (V_H) is the space between the top of the displacer piston and cylinder head. The cylinder head is stationary, while the displacer piston top moves with the crank angle based on drive mechanism. Cold volume (V_C) is the space between the bottom of displacer piston and the top of power piston, both of which move within the cylinder. Volumes are the product of the cross-section areas and the heights at each space. While the cross-section area of hot volume is equal to that of displacer pistons, the cross-section area of the cold volume is smaller as that of the displacer rod.

Depending on mechanism, the heights at each space vary with crank angle. The distances between the connection points and the top/bottom of pistons are considered the same for both mechanisms. The schematic views and dimensional descriptions of both mechanisms are given in Fig. 4. In crank drive mechanism, the distance between piston pin (B) and the crank axis (O) can be determined from Eq. (3) depending on crank angle (θ). Since it is a widely known mechanism, no more details were needed. Where r_c and l_c are the crank radius and the connecting rod length, respectively.

$$\overline{OB}_c = r_c\cos\theta + l_c\cos\left[\operatorname{asin}\left(\frac{r_c}{l_c}\sin\theta\right)\right] \tag{3}$$

Hypocycloid mechanism consists of the ring gear, planet gear and crank (also known as the carrier). The planet gear is in contact with the ring

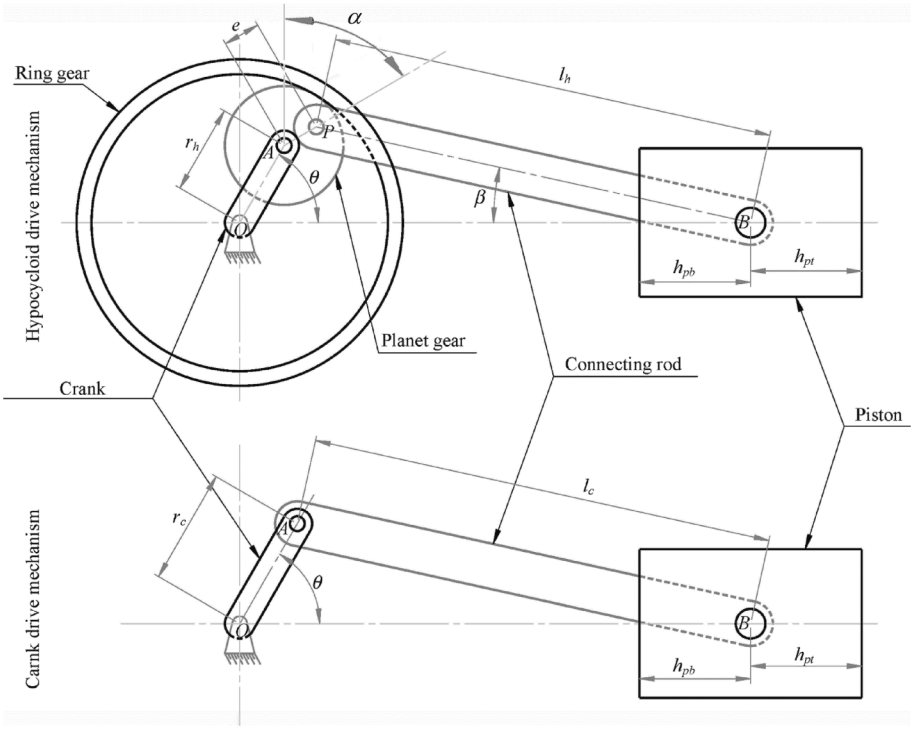

Fig. 4. Kinematic relations and descriptions of mechanisms.

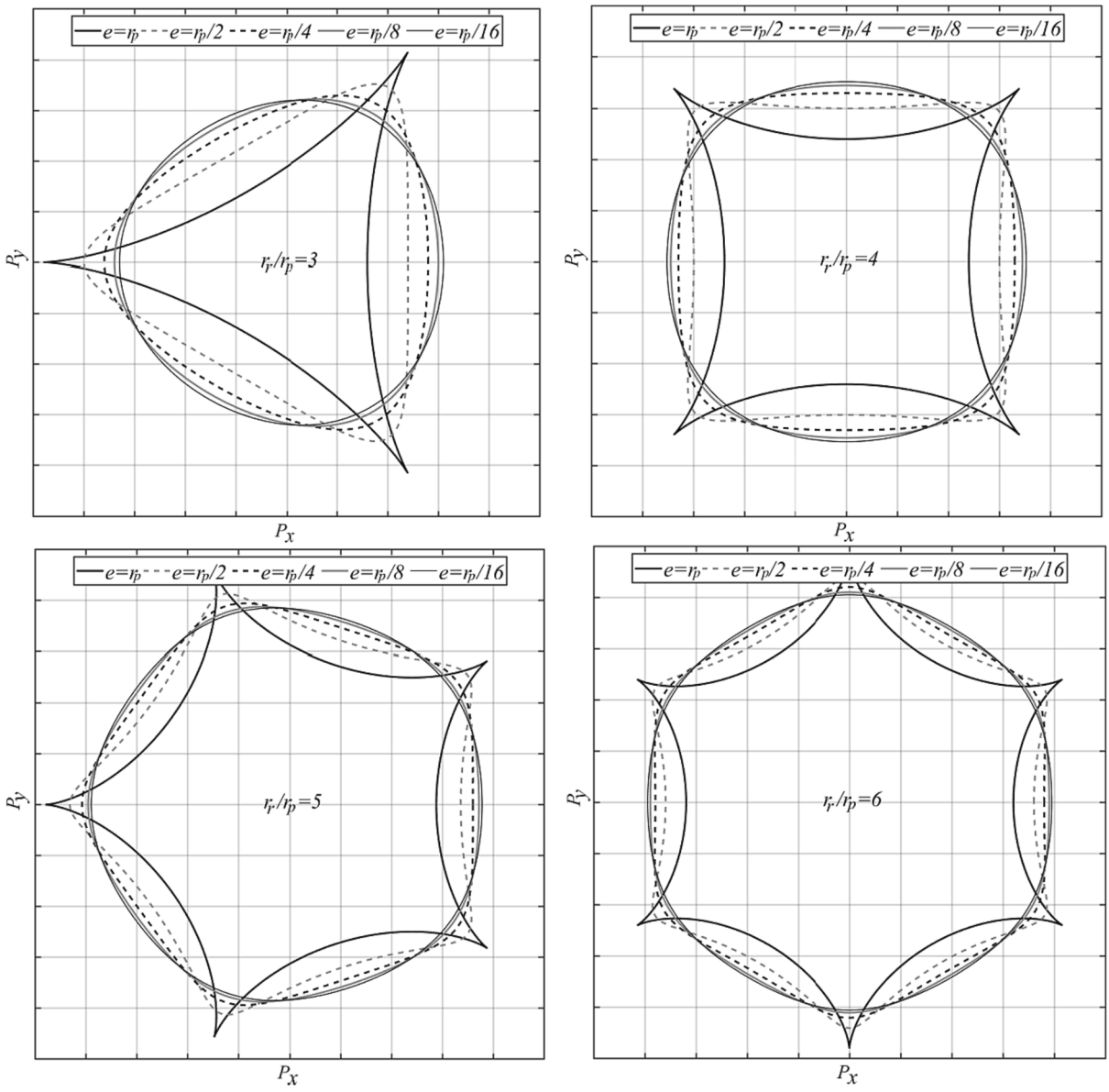

Fig. 5. Hypocycloid curve samples for different r_r/r_p ratios and e eccentricities.

gear and positioned on the crank pin. During the angular movement of the crank, it rotates around both the crank axis and own axis. Thus, an off-axis point on the planet gear (P point in Fig. 4) creates different hypocycloid curves depending on the eccentricity (e), the radius of planet gear (r_p) and the radius of ring gear (r_r). Hypocycloid curves can be achieved in $r_r > r_p$. The crank radius for hypocycloid drive mechanism (r_h) is equal to the difference of both gear radii (r_r - r_p). The coordinates of point P can be determined as in Eq. (4) [58]. In this equation, α is used to shift the hypocycloid curve phase angle.

$$\begin{matrix} P_x \\ P_y \end{matrix} = \begin{matrix} (r_r - r_p)\cos\theta + e\cos\left(\frac{r_r - r_p}{r_p}\theta + \alpha\right) \\ (r_r - r_p)\sin\theta - e\sin\left(\frac{r_r - r_p}{r_p}\theta + \alpha\right) \end{matrix} \quad (4)$$

Hypocycloid curves obtained for a few r_r/r_p integer ratios and e values are given in Fig. 5. It can be seen from figure that the different cusped forms occur in different ratios. The radius of concave arc between two cusps is almost constant and alters with r_r/r_p ratio. As r_r/r_p ratio increases, both of concave radius and arc length decrease. The concave arc length is important to set the piston dwell duration. The e value differs from the r_p leads to increase in the concave arc radius and to disappearance of the sharp edges. When e value gets too small, the concavity decreases and even the convex curves appear. The convex forms also enable the piston dwell in the opposite directions.

Table 1
The common dimensions of mechanisms.

Parameters	Value	Unit
Crank radius for crank mechanism	0.03	m
Connecting rod length of displacer piston	0.08	m
Connecting rod length of power piston	0.2	m
Cross-section area of cylinder	0.00385	m^2
Cross-section area of displacer rod	0.0002	m^2
Displacer rod length	0.315	m
Distances to piston pin of piston top and bottom	0.075	m
Total regenerator volume	0.0001	m^3

Location of the piston pin in hypocycloid drive was founded by using Eq. (5). The top and bottom locations of pistons vary with a fixed distance from the piston pins as in Eq. (6). These fixed distances were taken the same value for both mechanisms and given in Table 1 together with

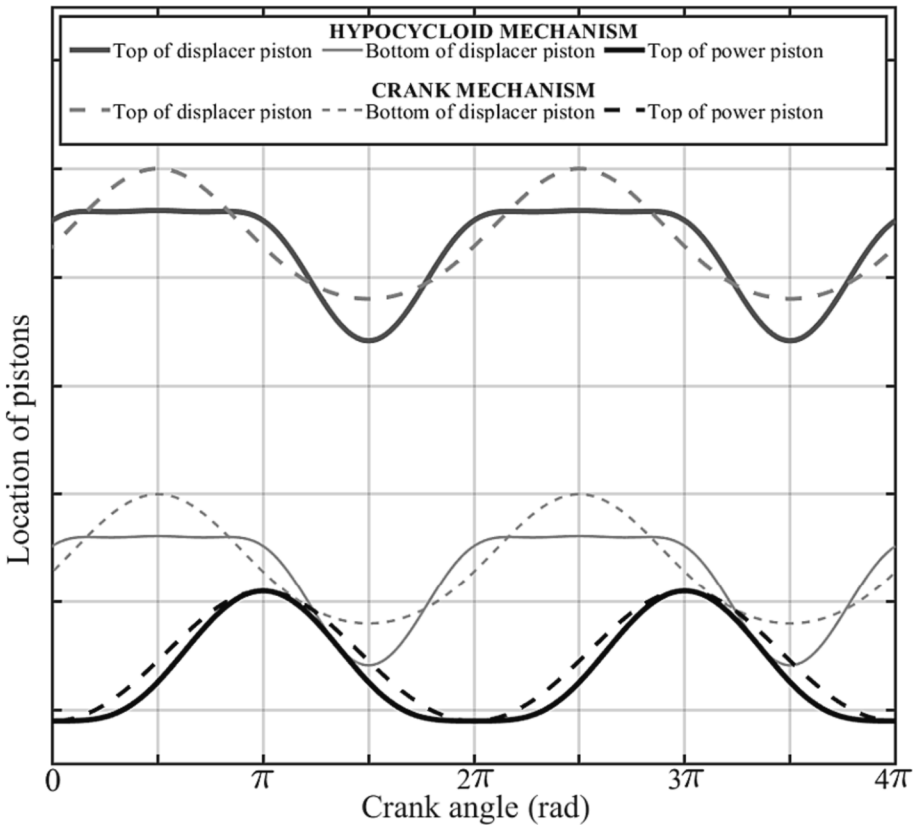

Fig. 6. The piston trajectories obtained with $r_r/r_p = 3$ hypocycloid curves.

the other parameters of mechanisms taken from ref. [55] for comparison with crank mechanism. In these equations, l_h and l_r are the connecting rod and displacer rod lengths, respectively. In cases of using the connecting rod length equal to the concave arc radius and bearing as coaxially to the cylinder axis of the arc center, piston will remain almost stationary in these regions. Piston dwell durations can also be changed with eccentricity (e) values.

$$\overline{OB}_h = P_x + l_h \cos\left[\operatorname{asin}\left(\frac{P_y}{l_h}\right)\right] \tag{5}$$

$$\begin{aligned} x_{pt} &= (\overline{OB}_h)_p + h_{pt} \\ x_{pb} &= (\overline{OB}_h)_p - h_{pb} \\ x_{dt} &= (\overline{OB}_h)_d + l_r + h_{pt} \\ x_{db} &= (\overline{OB}_h)_d + l_r - h_{pb} \end{aligned} \tag{6}$$

The locations of displacer piston top and bottom (x_{dt} and x_{db}) as well as power piston top (x_{pt}) can be seen in Fig. 6 compared with the crank drive mechanism. In this application example, the hypocycloid curves with $r_r/r_p = 3$ were used. The α phase angle and e eccentricity value of displacer piston were chosen as π and equal to r_p for an approximation to ideal cycle trajectories, respectively. These values were taken as π and $r_p/4$ for the power piston with the intention of dwelling in BDC region. The r_r value was specified as providing the same total swept volume with crank mechanism. When compared with Fig. 1, it can be seen that the hypocycloid mechanism yields a closer trajectory to ideal form. However, the regenerative heating (2–3 isochoric process in Fig. 1) was not sufficiently achieved due to the power piston motion at TDC (π rad). Additionally, the dwell duration of displacer piston at TDC is too long (about π rad), which adversely affects the isothermal expansion and isochoric cooling processes. These deficiencies uncovered the fact that the mechanism should be optimized to approach the ideal cycle.

5. Optimization procedure

The purpose of this study is to design a mechanism that will provide the ideal cycle volume change for the beta type Stirling engine without compromising from the specific power. As seen in Fig. 1, isochoric processes for the ideal cycle occur at the dwell periods of power piston, while the isothermal processes occur at the dwell period of displacer piston or the co-movement period of both pistons. It was mentioned in previous section that the dwelling of pistons can be partially ensured with the connecting rod lengths equal to the concave arc radius of hypocycloid curve. However, the dwell durations must also be optimized with regard to the thermodynamically behavior of system. The r_r/r_p ratios and e eccentricity values of each piston must be taken into account for the optimization of dwell durations. An inherent case of the beta type Stirling engine is the difference in cross-section areas at cold and hot volume regions based on displacer piston rod, which negatively affects the isochoric processes. The α phase angle for only power piston can be used to eliminate this negative effect. These five variables were optimized for the hypocycloid drive mechanism.

In the optimization, five objective functions were used to minimize the volume variations of two isochoric and two isothermal processes as well as to maximize the cyclic work. The variations depending on crank angle of V_H, V_C and total volumes (V_T) were obtained from Eq. (7). Where, l_{ch}, V_R, A_{cs} and A_{dr} have a fixed value and represent the distance between the crank axis and cylinder head, the regenerator volume, the cylinder cross section and displacer rod areas, respectively.

$$\begin{aligned} V_H &= A_{cs}(l_{ch} - x_{dt}) \\ V_C &= (A_{cs} - A_{dr})(x_{db} - x_{pt}) \\ V_T &= V_H + V_C + V_R \end{aligned} \tag{7}$$

Isochoric cooling process (4–1 in Fig. 1) is regarded as 1st objective function. In this process that matches from 7π/4 to 9π/4 in Fig. 6, the variation of V_T - V_R (or $V_H + V_C$) must be zero. This circumstance is also

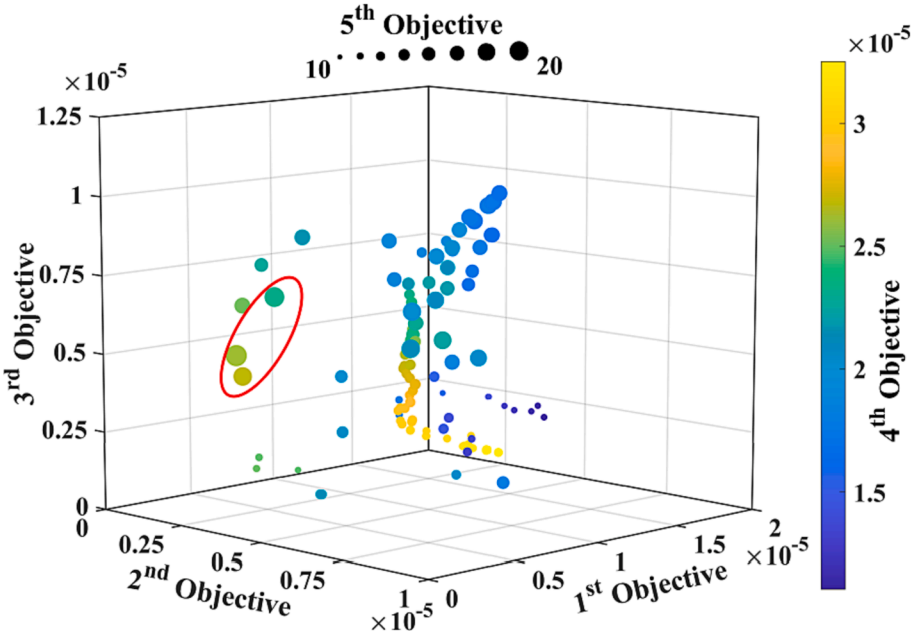

Fig. 7. Pareto frontier results of optimization with five optimize variables.

valid for the isochoric heating process (2–3 in Fig. 1 and the between 3π/4 and 5π/4 in Fig. 6) which considered as 2nd objective function. The 3rd objective function is for the isothermal compression (1–2 in Fig. 1). Within this period that coincides with the crank interval from π/4 to 3π/4 in Fig. 6, the V_H must be zero. In the isothermal expansion process (3–4 in Fig. 1) which is regarded as the 4th objective function, V_C must be zero for the crank interval from 5π/4 to 7π/4. Even though it is not expected to be zeroed of the all objective functions, the decrease of variations within these specified periods can be ensured. For this purpose, the minimization procedure given in Eq. (8) can be used in the optimization of objective functions related to volumes. The RSS method was used to consider the deviations of the negative and positive values. The 5th optimization function is for the cyclic work given in Eq. (2). The equation of cyclic work is used with its opposite sign to compose the minimize function.

$$f_{obj1^{st}} = min\left(\sqrt{\sum\left(\frac{dV_T\left(r_{rd}/r_{pd}, r_{rp}/r_{pp}, e_d, e_p, \alpha\right)}{d\theta}\right)^2}\right), 7\pi/4 \rightarrow 9\pi/4$$

$$f_{obj2^{nd}} = min\left(\sqrt{\sum\left(\frac{dV_C\left(r_{pd}/r_{rd}, r_{rp}/r_{pp}, e_d, e_p, \alpha\right)}{d\theta}\right)^2}\right), 3\pi/4 \rightarrow 5\pi/4$$

$$f_{obj3^{rd}} = min\left(\sqrt{\sum\left(\frac{dV_T\left(r_{rd}/r_{pd}, r_{rp}/r_{pp}, e_d, e_p, \alpha\right)}{d\theta}\right)^2}\right), \pi/4 \rightarrow 3\pi/4$$

$$f_{obj4^{th}} = min\left(\sqrt{\sum\left(\frac{dV_H\left(r_{rd}/r_{pd}, r_{rp}/p, e_d, e_p, \alpha\right)}{d\theta}\right)^2}\right), 5\pi/4 \rightarrow 7\pi/4$$

$$f_{obj5^{th}} = min\left(-\oint pdV\right), 0 \rightarrow 2\pi \tag{8}$$

The different r_r/r_p gear ratios for both pistons were used to provide the same swept volume and compression ratio with the crank mechanism. The r_{rd}/r_{pd} gear ratio for displacer piston and r_{rp}/r_{pp} for power piston must be positive integers. In order to get the piston dwelling, these gear ratios must be higher than 2 which generate only sinusoidal motions. Also, the dwell durations may be insufficient above r_r/r_p ratio of 6. These values were treated as the lower and upper bonds of r_r/r_p ratios. The eccentricity values (e_d and e_p) of displacer and power pistons must be higher than zero and lower than r_{pd} and r_{pp} values, respectively. Power piston phase angle (α) was optimized with π/180 rad precision from 5π/6 to 10π/9 rad. Thus, α also was considered as integer after derived from radian to degree. Besides the integer and non-integer optimization variables, this problem having five objective functions contains also non-linear equations. Therefore, the optimization problem is in the multi objective classification with mixed variables.

When numerous criteria are included in the decision-making process, multi-objective optimization is beneficial [59]. The genetic algorithm approach is a good choice for the solution of non-linear equations, although it does not guarantee an absolute solution [60,61]. The NSGA-II is a genetic algorithm that is an upgraded version of the NSGA. A function based on NSGA-II of MATLAB, '*gamultiobj*' was implemented to detect the suitable solutions. No constraint functions could be used because the optimization routine contains integer variables, which are intrinsic to the optimization function used. The optimization results were analyzed on Pareto optimal set, and the best solutions were selected by comparing with the others.

The optimization process was carried out on a PC with an i7 processor and 8 GB RAM. Since the analysis for each case was calculated according to the same swept volume and compression ratio with the crank mechanism and no constraint function could be used, the first optimization procedure took 5 h and 48 min. For the second optimization procedure, 3 h and 17 min were sufficient, thanks to the lack of two optimized parameters.

6. Results and discussions

Hypocycloid drive mechanism offered in present study was compared with the crank mechanism under the same swept volume and compression ratio, as commonly considered in the literature [32,35,53]. To obtain the same values, the values of planet gear radius of both pistons (r_{pd} and r_{pp}) were numerically computed in a subroutine of objective function. Except for the drive mechanisms, other parameters were taken equal to each other as in Table 1.

Pareto frontiers obtained with the 200 population size at a fraction of 0.5 are given in Fig. 7. The 3rd and 4th objectives deteriorated in regions where the optimal results were obtained for 1st and 2nd objectives. Moreover, optimal results for both 3rd and 4th objectives were obtained

Table 2
The 12 optimal results selected from Pareto frontier as base on the cyclic work.

	Objective Successions (x 10^{-6})					Optimize Variables				
	1st	2nd	3rd	4th	5th	r_{rd}/r_{pd}	r_{rp}/r_{pp}	e_d (mm)	e_p (mm)	α (deg)
1	**2.6321**	3.0330	5.1438	26.078	**19.572**	5	4	4.60	6.01	179
2	3.9235	2.9070	7.1999	23.231	19.078	5	4	2.51	4.59	174
3	3.0933	**2.5570**	**4.6038**	26.748	18.667	5	4	5.99	5.28	185
4	6.7518	5.4477	5.8425	21.211	18.625	5	4	4.02	1.60	178
5	6.8418	5.3473	7.0072	20.106	18.536	5	4	2.81	1.61	190
6	4.5162	11.859	5.2193	22.326	18.348	5	3	4.48	4.88	185
7	3.8046	12.839	6.3309	20.904	18.156	5	3	3.22	6.20	176
8	7.1746	8.3885	9.6344	**17.039**	18.106	3	5	2.24	1.09	189
9	7.2552	8.4950	5.3853	20.419	17.998	5	3	4.50	1.29	178
10	8.0399	6.3353	9.9913	17.488	17.907	6	4	0.81	0.51	166
11	7.8229	7.8670	10.218	17.546	17.904	3	3	1.09	1.10	195
12	8.4633	6.8291	10.480	17.245	17.887	3	6	0.61	0.27	198

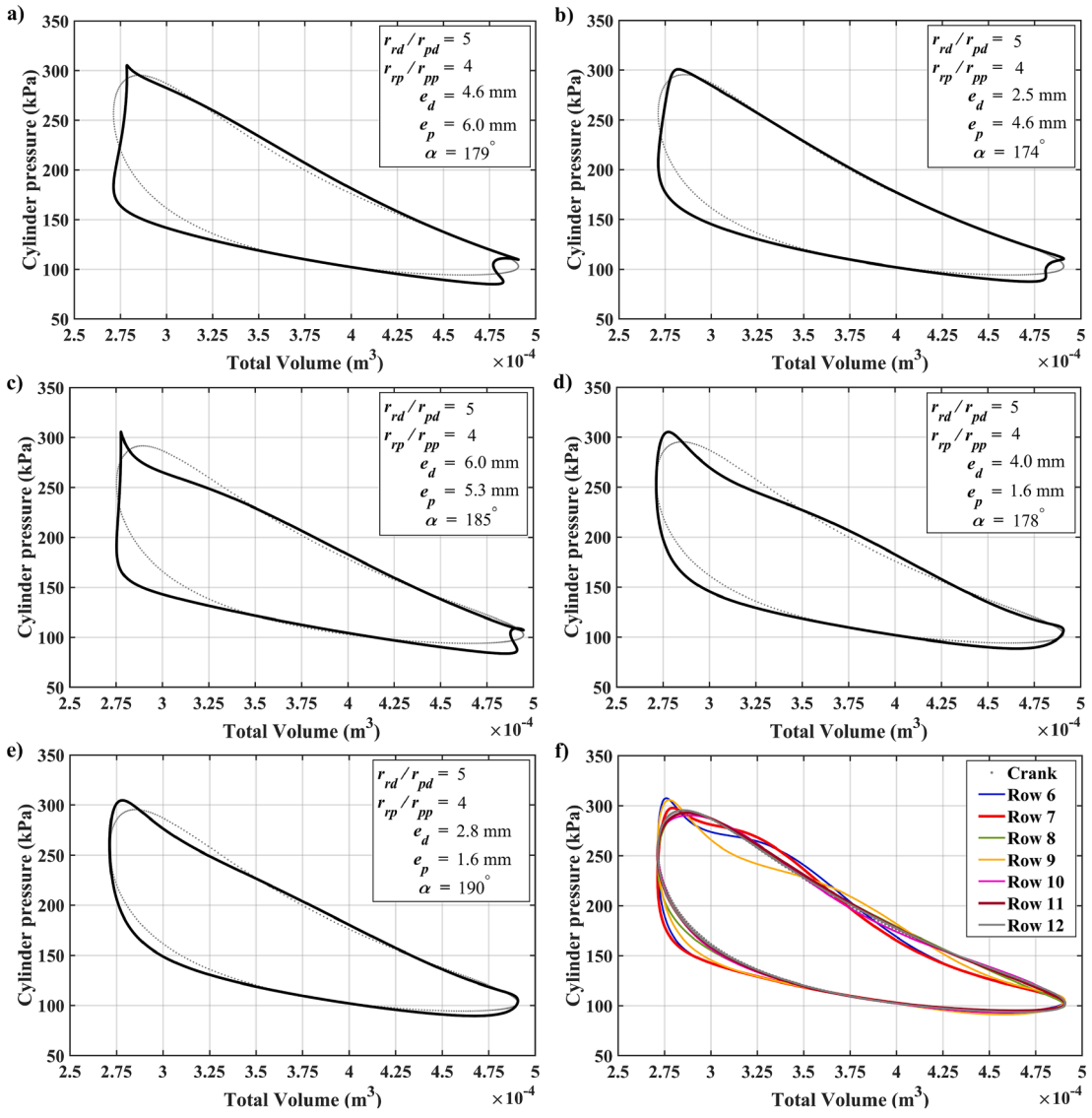

Fig. 8. The comparison of PV diagrams for optimal ring/planet gear ratio combination.

in the deteriorated regions of 1st and 5th. Marker size represents the 5th objective function results and these results were graphed in a manner consistent with the purpose to increase the cyclic work. Therefore, larger marker sizes indicate more ideal results. It can be seen from Fig. 7 that three greatest cyclic works (encircled with red oval) are collected in the region where the 1st and 2nd objectives are optimum, but 3rd and 4th objectives are mid-range. None of objective functions gave better results without worsening another one or more. In multi objective optimizations, decision-makers can select the best satisfies among Pareto frontier solutions [61,62]. The cyclic work of crank mechanism used for comparison in this study is 17.635 J. The lower cyclic works are corresponding to the lower specific powers. Thus, the 12 optimal results

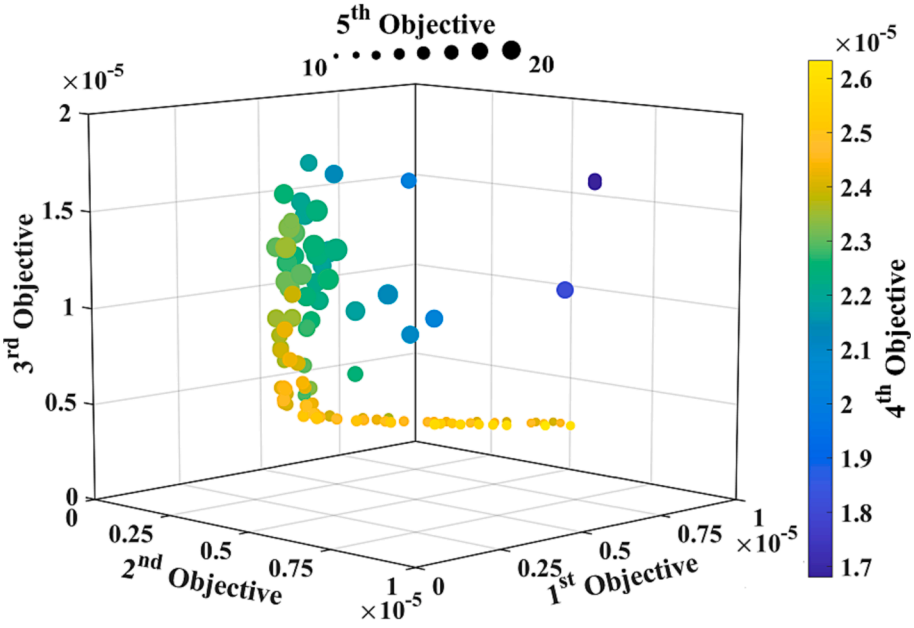

Fig. 9. Pareto frontier results of optimization with three optimize variables.

having the higher cyclic work than that of the crank mechanism, besides the approximation performance to ideal Stirling Cycle trajectories, were selected and given in Table 2. The best successions for each objective were marked bold in Table. As can be seen, the maximum cyclic works and the minimum volume variations along isochoric processes (1st and 2nd objectives) were obtained with 5 and 4 gear ratios of displacer and power pistons, respectively. Also, the two optimize parameters (1. and 3. rows in Table 2) including this gear ratio combination have the best successions for 3rd objective (isothermal compression) and the worst for 4th objective (isothermal expansion).

Except the isothermal expansion approximation (4th objective), the other requirements for the ideal Stirling cycle were achieved with the ring/planet gear ratios of 5 for displacer piston and of 4 for power piston. The P-V indicator diagrams individually for this gear ratio combination and all together for other gear ratios were presented comparatively with the crank mechanism (drawn with dotted lines) in Fig. 8.

When examining Fig. 8.a and b, it was seen that the isothermal compression process occurred better than those of crank mechanism, while isothermal expansion processes are quite close to each other. Moreover, the volume oscillations in isochoric regions increased due to the excessive eccentricity values, especially for isochoric cooling process. There was a similar situation also in Fig. 8.c while it was not seen for the lower e_p value (Fig. 8.d and e). As both eccentricity values decrease, the PV indicator diagrams and thereby the cyclic works closed to the crank mechanism that exhibits near-sinusoidal motion. The optimal isochoric process was obtained with high e eccentricity and α phase angle values. The isochoric heating process occurred at almost constant volume for phase angle of 185° as can be seen from Fig. 8.c. It is seen from Fig. 8.f that the gear ratios that stay out of the chosen combination have the low cyclic works and successions especially for the isochoric cooling process.

These results show that the hypocycloid gear mechanism with the gear ratio combinations r_{rd}/r_{pd} of 5 and r_{rp}/r_{pp} of 4 is a suitable approach. However, the increase in number of objective functions and variables may cause to the rising trade-off solutions that include local optimums and thus miss the more accurate results. In order to obtain more optimal results, the optimized variable number should be reduced [63,64]. The second optimization procedure was implemented to find only the optimum eccentricity values (e_d and e_p) and phase angle (α) by reducing the variable number from 5 to 3. Pareto frontier graph of second optimization was obtained by using the same functions and bounds as in the first optimization, and given in Fig. 9. As in the previous optimization, the highest cyclic works are collected in the optimal regions of the 1st

Table 3
The best succession samples selected from the second optimization results.

	Objective Successions (x 10^{-6})					Optimize Variables		
	1st	2nd	3rd	4th	5th	e_d (mm)	e_p (mm)	α (deg)
1st	**2.6267**	3.0653	13.087	23.023	19.191	4.54	5.43	186
	2.6281	3.4999	11.331	22.698	19.274	3.55	4.93	183
	2.6654	3.5658	12.522	22.453	19.397	4.20	4.81	181
2nd	3.7309	**2.2756**	9.2946	24.225	17.976	2.49	**6.78**	188
	3.9054	**2.3488**	11.127	23.914	18.223	3.49	**6.97**	192
	3.7398	**2.4892**	11.031	23.437	18.012	3.43	**6.73**	195
3rd	3.1415	4.9640	**6.0932**	22.502	17.752	**0.49**	3.63	183
	3.0146	2.8102	**7.9016**	23.786	17.819	**1.69**	5.91	188
	2.8338	2.9899	**7.9136**	23.620	18.044	**1.66**	5.55	182
4th	6.7269	7.9381	10.681	**18.132**	18.294	3.13	**0.39**	182
	4.2838	5.5077	16.366	**20.123**	17.711	6.35	**2.72**	186
	4.4433	6.1444	9.0545	**20.388**	18.548	2.25	**2.36**	191
5th	3.6435	3.9085	12.989	22.305	**20.133**	4.39	5.12	**162**
	3.3342	3.5332	13.209	22.479	**20.010**	4.52	5.27	**167**
	3.2787	3.6810	12.719	22.387	**19.964**	4.26	5.04	**167**

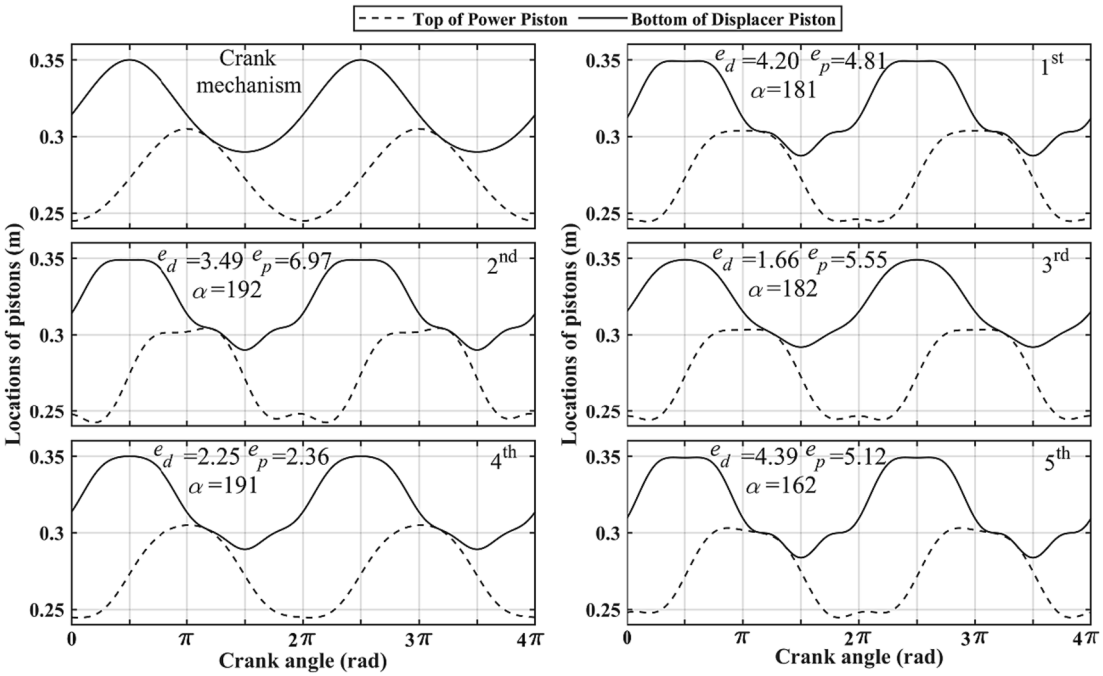

Fig. 10. Piston trajectories correspond to the higher cyclic work of each objective.

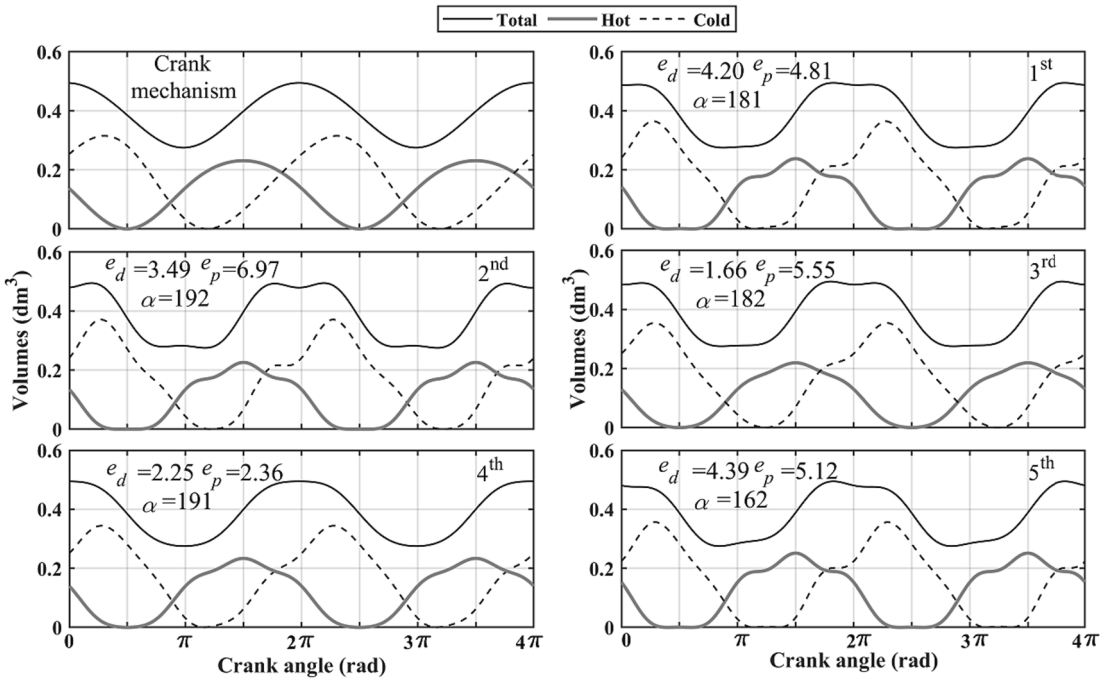

Fig. 11. The volume variations correspond to the higher cyclic work of each objective.

and 2nd objectives. Although no significant change is seen in the 3rd and 4th objectives in comparison with the previous optimization, this optimization routine resulted in the more optimal points of 44 samples having the higher cyclic works than the crank mechanism. The best three successions for each objective were chosen between these samples and presented in Table 3. There seems to be certainty in the ranges of some optimize variables for each objective succession, individually.

The ranges of e_d, e_p and α are 0.49–6.35, 0.39–6.97 and 162–195 for all samples in Table 3, respectively. The best results for 3rd objective were obtained with the low e_d values, but no obvious results were observed for the 1st objective. However, the best successions for 2nd objective occurred at the high e_p, whereas vice versa for 4th. The fact that the high values of objective 5 originated at low α values is an obvious case. Another outstanding case is that the α values below 180° (π rad) are optimal with regard to the cyclic work (5th objective succession), while the above 180° are optimal for other objectives. In order to detail the findings, the optimize variables having the highest cyclic works specific to each objective succession were compared in Figs. 10–12. In Fig. 10, the trajectories of pistons are given as comparatively with crank mechanism. Also, Figs. 11 and 12 are the volume variations and PV indicator diagrams, respectively.

It can be seen from Fig. 10 that except of the displacer piston for 5th

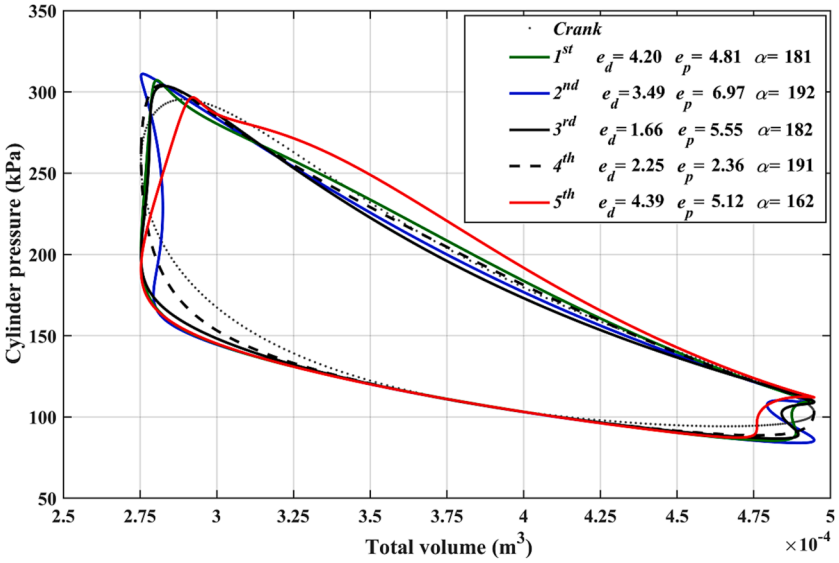

Fig. 12. PV indicator diagrams of ideal results with regards to the cyclic work.

objective succession, the strokes of pistons are almost the same with the crank mechanism. The piston dwell periods of hypocycloid mechanism are longer than that of crank mechanisms. Low eccentricity values reduced the dwelling of pistons whereas high values caused to the piston oscillations at the isochoric periods. As can be seen form Fig. 11, the increase in e_d value enhanced the isothermal compression process by zeroing the hot volume. Although the zeroing of cold volume was also provided with the high e_d, this period which was expected to occur at the crank interval 5π/4-7π/4 advanced to the interval π-3π/4. At the same time, this could be seen as the main reason for the deficiency of 4th objective succession in proportion to other objectives. The excessive e_p values caused to the volume oscillations, especially for the isochoric cooling period. As the α value moves away from 180°, the power piston has not remained stationary at both dwelling periods. In this study, the main purpose of phase angle (α) is to tolerate the volume variations arising from the piston rod cross-section area at isochoric periods. While this purpose was achieved with the high α values, the isochoric periods were negatively affected from the decrease of α as seen from Fig. 11. These cases can be examined from the total volume regions that correspond to π and multiples in Fig. 11.

According to the PV indicator diagrams in Fig. 12, the highest value of maximum in-cylinder pressure was obtained at the best 2nd objective succession (isochoric heating). Despite the fact that the lowest in-cylinder pressure was expected to occur in 1st objective succession (isochoric cooling), it also occurred in the 2nd objective. This result can be explained by a faster increase in cold volume for the case of 2nd objective succession. For the 1st, 2nd, 3rd and 5th objective successions, the PV curves are nearly identical at the majority of isothermal compression region. However, PV curves diverged at the isothermal expansion regions. This divergence can be attributed to the low successions in 4th objective. The greater indicated work area was obtained at the 5th objective succession. Even if it does not occur at the appropriate period of cycle, the overlapping of pistons at beginning of isothermal expansion period minimized the decrease in pressure by providing both the more hot space and the less cold space volumes in comparison with the others.

The proposed mechanism in this study failed only for the isothermal expansion period. However, higher cyclic works were achieved than crank mechanism. The maximum increase of 14 % was obtained at the 5th objective. Except the 4th and 5th objective, 1st objective having the better successions in terms of other objectives was ranked second with a work increment of 10 %. Similar results on the cyclic work increment with isochoric periods can be seen in Refs. [27,35,36]. These results presented that the improvement in the power can be accomplished by approaching the ideal Stirling cycle, but still and all the achieved maximum power is in some out of ideal case.

7. Conclusion

This paper presents a novel drive mechanism for the beta type Stirling engines. This novel mechanism is based on hypocycloid curves. The appropriate curves for pistons were obtained by optimizing the parameters of hypocycloid drive mechanism. This mechanism is perfectly capable of dwelling the pistons, but insufficient for the piston overlapping of in expected period. Also, mechanism has the potential to produce more cyclic work than crank mechanism with the same swept volume and compression ratio. The main findings on ideal Stirling cycle approach of present work are listed as follows:

- The isochoric heating and cooling processes influenced positively the cyclic work and thus the power. The isochoric processes for a beta type Stirling engine can be provided with the dwelling of power piston at both TDC and BDC.
- The high eccentricity values for the power piston increased the dwelling duration while the excessive amount caused the oscillations at volume. The phase angle can be used to minimize the volume variations arising from the displacer rod cross-section area unique to the beta type.
- The compression with the zero hot volume also increased the cyclic work. The dwelling of displacer piston at TDC procures the zeroing of hot volume for beta type Stirling engines. The high eccentricity value of displacer piston not only increases the durations of piston dwell but also enhances the overlap period.
- Because the zeroing cold volume cannot be sufficiently achieved in any cases of the hypocycloid drive mechanism, no marked result is obtained for the expansion with the zero cold volume. However, the low cold volumes during expansion period enhanced the cyclic work.
- On the other hand, the highest cyclic works were observed in cases that not exactly ideal but were close.

For future studies, the optimization of hypocycloid drive mechanism for the different Stirling engine configurations would be interesting. Also, this work was restricted to the same dimensional parameters for a correct comparison with crank mechanism. The more ideal cycle successions and higher cyclic works may be obtained by optimizing other mechanism parameters, regardless of comparison.

8. Statements and declarations

The authors declare that they have no known competing financial interests or personal relationships that could have appeared to influence the work reported in this paper.

Declaration of Competing Interest

The authors declare that they have no known competing financial interests or personal relationships that could have appeared to influence the work reported in this paper.

References

[1] C.H. Cheng, D.T. Phung, Numerical and experimental study of a compact 100-W-class β-type Stirling engine, Int. J. Energy Res. 45 (2021) 6784–6799, https://doi.org/10.1002/er.6271.
[2] O. Farhat, J. Faraj, F. Hachem, C. Castelain, M. Khaled, A recent review on waste heat recovery methodologies and applications: Comprehensive review, critical analysis and potential recommendations, Clean. Eng. Technol. 6 (2022), 100387, https://doi.org/10.1016/j.clet.2021.100387.
[3] V. İncili, G. Karaca Dolgun, A. Georgiev, A. Keçebaş, N.S. Çetin, Performance evaluation of novel photovoltaic and Stirling assisted hybrid micro combined heat and power system, Renew. Energy 189 (2022) 129–138, https://doi.org/10.1016/j.renene.2022.03.030.
[4] O. Erixno, N.A. Rahim, F. Ramadhani, N.N. Adzman, Energy management of renewable energy-based combined heat and power systems: A review, Sustain. Energy Technol. Assess. 51 (2022), 101944, https://doi.org/10.1016/j.seta.2021.101944.
[5] A. Dik, S. Omer, R. Boukhanouf, Electric Vehicles: V2G for Rapid, Safe, and Green EV Penetration, Energies 15 (2022), https://doi.org/10.3390/en15030803.
[6] S.M. Alirahmi, E. Assareh, N.N. Pourghassab, M. Delpisheh, L. Barelli, A. Baldinelli, Green hydrogen & electricity production via geothermal-driven multi-generation system: Thermodynamic modeling and optimization, Fuel 308 (2022), 122049, https://doi.org/10.1016/j.fuel.2021.122049.
[7] M. Çeçen, C. Yavuz, C.A. Tırmıkçı, S. Sarıkaya, E. Yanıkoğlu, Analysis and evaluation of distributed photovoltaic generation in electrical energy production and related regulations of Turkey, Clean Techn. Environ. Policy (2022), https://doi.org/10.1007/s10098-021-02247-0.
[8] Z. Wang, Z. Wu, Z. Hu, J. Orrego-Hernández, E. Mu, Z.-Y. Zhang, M. Jevric, Y. Liu, X. Fu, F. Wang, T. Li, K. Moth-Poulsen, Chip-scale solar thermal electrical power generation, Cell Rep. Phys. Sci. 3 (2022), 100789, https://doi.org/10.1016/j.xcrp.2022.100789.
[9] A. Azarpour, S. Suhaimi, G. Zahedi, A. Bahadori, A review on the drawbacks of renewable energy as a promising energy source of the future, Arab. J. Sci. Eng. 38 (2013) 317–328, https://doi.org/10.1007/s13369-012-0436-6.
[10] H. Karabulut, C. Çinar, E. Oztürk, H.S. Yücesu, Torque and power characteristics of a helium charged Stirling engine with a lever controlled displacer driving mechanism, Renew. Energy 35 (2010) 138–143, https://doi.org/10.1016/j.renene.2009.04.023.
[11] U.R. Singh, A. Kumar, Review on solar Stirling engine: Development and performance, Therm. Sci. Eng. Prog. 8 (2018) 244–256, https://doi.org/10.1016/j.tsep.2018.08.016.
[12] D.G. Thombare, S.K. Verma, Technological development in the Stirling cycle engines, Renew. Sustain. Energy Rev. 12 (2008) 1–38, https://doi.org/10.1016/j.rser.2006.07.001.
[13] D. Erol, S. Çalışkan, The examination of performance characteristics of a beta-type Stirling engine with a rhombic mechanism: The influence of various working fluids and displacer piston materials, Int. J. Energy Res. 45 (2021) 13726–13747, https://doi.org/10.1002/er.6702.
[14] H. Hachem, R. Gheith, F. Aloui, S., Ben Nasrallah, Technological challenges and optimization efforts of the Stirling machine: A review, Energy Convers. Manag. 171 (2018) 1365–1387, https://doi.org/10.1016/j.enconman.2018.06.042.
[15] D. Ipci, H. Karabulut, Thermodynamic and dynamic analysis of an alpha type Stirling engine and numerical treatment, Energy Convers. Manag. 169 (2018) 34–44, https://doi.org/10.1016/j.enconman.2018.05.044.
[16] H. Karabulut, M. Okur, S. Halis, M. Altin, Thermodynamic, dynamic and flow friction analysis of a Stirling engine with Scotch yoke piston driving mechanism, Energy 168 (2019) 169–181, https://doi.org/10.1016/j.energy.2018.11.078.
[17] M. Altin, M. Okur, D. Ipci, S. Halis, H. Karabulut, Thermodynamic and dynamic analysis of an alpha type Stirling engine with Scotch Yoke mechanism, Energy 148 (2018) 855–865, https://doi.org/10.1016/j.energy.2018.01.183.
[18] K. Wang, S. Dubey, F.H. Choo, F. Duan, A transient one-dimensional numerical model for kinetic Stirling engine, Appl. Energy 183 (2016) 775–790, https://doi.org/10.1016/j.apenergy.2016.09.024.
[19] Y. Timoumi, I. Tlili, S., Ben Nasrallah, Design and performance optimization of GPU-3 Stirling engines, Energy 33 (2008) 1100–1114, https://doi.org/10.1016/j.energy.2008.02.005.
[20] D. Erol, H. Yaman, B. Doğan, A review development of rhombic drive mechanism used in the Stirling engines, Renew. Sustain. Energy Rev. 78 (2017) 1044–1067, https://doi.org/10.1016/j.rser.2017.05.025.
[21] S. Kojima, Maximum Work of Free-Piston Stirling Engine Generators, J. Non-Equilibrium Thermodyn. 42 (2017) 169–186, https://doi.org/10.1515/jnet-2016-0031.
[22] J.E. Shaw, Comparing Carnot, Stirling, Otto, Brayton and Diesel Cycles, Trans. Missouri Acad. Sci. 42 (2008) 1–6, https://doi.org/10.30956/0544-540x-42.2008.1.
[23] S. Ranieri, G.A.O. Prado, B.D. MacDonald, Efficiency reduction in stirling engines resulting from sinusoidal motion, Energies 11 (2018) 1–14, https://doi.org/10.3390/en11112887.
[24] M. Scheunert, R. Masser, A. Khodja, R. Paul, K. Schwalbe, A. Fischer, K. H. Hoffmann, Power-optimized sinusoidal piston motion and its performance gain for an alpha-type stirling engine with limited regeneration, Energies 13 (2020), https://doi.org/10.3390/en13174564.
[25] R. Masser, A. Khodja, M. Scheunert, K. Schwalbe, A. Fischer, R. Paul, K. H. Hoffmann, Optimized piston motion for an alpha-type stirling engine, Entropy 22 (2020) 1–19, https://doi.org/10.3390/e22060700.
[26] R. Paul, A. Khodja, A. Fischer, R. Masser, K.H. Hoffmann, Power-Optimal Control of a Stirling Engine's Frictional Piston Motion, Entropy 24 (2022) 362, https://doi.org/10.3390/e24030362.
[27] J. Bert, D. Chrenko, T. Sophy, L. Le Moyne, F. Sirot, Simulation, experimental validation and kinematic optimization of a Stirling engine using air and helium, Energy 78 (2014) 701–712, https://doi.org/10.1016/j.energy.2014.10.061.
[28] R. Paul, K.H. Hoffmann, Cyclic control optimization algorithm for stirling engines, Symmetry (basel). 13 (2021), https://doi.org/10.3390/sym13050873.
[29] A. Della Torre, A. Guzzetti, G. Montenegro, T. Cerri, A. Onorati, F. Aloui, CFD modelling of a beta-type stirling machine, 11th World Congr. Comput. Mech. WCCM 2014, 5th Eur. Conf. Comput. Mech. ECCM 2014 6th Eur. Conf. Comput. Fluid Dyn. ECFD 2014. (2014) 1096–1113.
[30] H. Tian, S. Zhao, Y. Gong, Study of piston trajectory parameters on the performance of a kinetic Stirling engine, Proc. Inst. Mech. Eng. Part A J. Power Energy. 236 (2022) 865–874, https://doi.org/10.1177/09576509221075483.
[31] M. Craun, B. Bamieh, Optimal periodic control of an ideal stirling engine model, J. Dyn. Syst. Meas. Control. Trans. ASME. 137 (2015) 1–10, https://doi.org/10.1115/1.4029682.
[32] M.H. Briggs, J. Prahl, K. Loparo, Improving power density of free-piston stirling engines, 14th Int, Energy Convers. Eng. Conf. 2016 (2016), https://doi.org/10.2514/6.2016-5016.
[33] B. Cullen, J. McGovern, Development of a theoretical decoupled Stirling cycle engine, Simul. Model. Pract. Theory 19 (2011) 1227–1234, https://doi.org/10.1016/j.simpat.2010.06.011.
[34] N. Boutammachte, J. Knorr, Field-test of a solar low delta-T Stirling engine, Sol. Energy 86 (2012) 1849–1856, https://doi.org/10.1016/j.solener.2012.03.001.
[35] H.M. Wong, S.Y. Goh, Experimental comparison of sinusoidal motion and non-sinusoidal motion of rise-dwell-fall-dwell in a Stirling engine, J. Mech. Eng. Sci. 14 (2020) 6971–6981, https://doi.org/10.15282/jmes.14.3.2020.01.0546.
[36] H. Karabulut, M. Okur, C. Cinar, Mechanical Configuration and Thermodynamic Analysis of an Alpha-Type Stirling Engine with Crank-Shifted Driving Mechanism, Iran. J. Sci. Technol. - Trans, Mech. Eng. (2021), https://doi.org/10.1007/s40997-021-00436-2.
[37] M. Nicol-Seto, D. Nobes, Experimental evaluation of piston motion modification to improve the thermodynamic power output of a low temperature gamma Stirling engine, E3S Web Conf. 313 (2021) 04002, https://doi.org/10.1051/e3sconf/202131304002.
[38] H.W. Fang, K.E. Herold, H.M. Holland, E.H. Beach, Novel Stirling engine with an elliptic drive, Proc. Intersoc. Energy Convers. Eng. Conf. 2 (1996) 1232–1237, https://doi.org/10.1109/iecec.1996.553887.
[39] S. Kota, Generic models for designing dwell mechanisms: A novel kinematic design of stirling engines as an example, J. Mech. Des. Trans. ASME 113 (1991) 446–450, https://doi.org/10.1115/1.2912803.
[40] D.J. Shendage, S.B. Kedare, S.L. Bapat, An analysis of beta type Stirling engine with rhombic drive mechanism, Renew. Energy 36 (2011) 289–297, https://doi.org/10.1016/j.renene.2010.06.041.
[41] M. Farid Zainudin, R. Abu Bakar, K. Al Kadirgama, G. Leong Ming, Kinematic and thermodynamic operational analysis of rhombic-drive Stirling engine prototype, IOP Conf, Ser. Mater. Sci. Eng. 788 (2020), https://doi.org/10.1088/1757-899X/788/1/012070.
[42] A. Sripakagorn, C. Srikam, Design and performance of a moderate temperature difference Stirling engine, Renew. Energy 36 (2011) 1728–1733, https://doi.org/10.1016/j.renene.2010.12.010.
[43] K. Laazaar, N. Boutammachte, New approach of decision support method for Stirling engine type choice towards a better exploitation of renewable energies, Energy Convers. Manag. 223 (2020), 113326, https://doi.org/10.1016/j.enconman.2020.113326.
[44] M. Güven, H. Bedir, G. Anlaş, Optimization and application of Stirling engine for waste heat recovery from a heavy-duty truck engine, Energy Convers. Manag. 180 (2019) 411–424, https://doi.org/10.1016/j.enconman.2018.10.096.
[45] P. Chen, P. Yang, L. Liu, Y. Liu, Parametric investigation of the phase characteristics of a beta-type free piston Stirling engine based on a thermodynamic-dynamic coupled model, Energy 219 (2021), 119658, https://doi.org/10.1016/j.energy.2020.119658.
[46] J. Egas, D.M. Clucas, Stirling engine configuration selection, Energies 11 (2018) 1–22, https://doi.org/10.3390/en11030584.
[47] M.H. Ahmadi, H. Sayyaadi, S. Dehghani, H. Hosseinzade, Designing a solar powered Stirling heat engine based on multiple criteria: Maximized thermal efficiency and power, Energy Convers. Manag. 75 (2013) 282–291, https://doi.org/10.1016/j.enconman.2013.06.025.

[48] F. Ahmed, H. Hulin, A.M. Khan, Numerical modeling and optimization of beta-type Stirling engine, Appl. Therm. Eng. 149 (2019) 385–400, https://doi.org/10.1016/j.applthermaleng.2018.12.003.
[49] H. Hachem, R. Gheith, F. Aloui, S. Ben Nasrallah, I. Dincer, Exergy assessment of heat transfer inside a Beta type Stirling engine, Int. J. Exergy 20 (2016) 186–202, https://doi.org/10.1504/IJEX.2016.076863.
[50] C. Dobre, L. Grosu, M. Costea, M. Constantin, Beta type stirling engine. Schmidt and finite physical dimensions thermodynamics methods faced to experiments, Entropy. 22 (2020) 1–15. doi:10.3390/e22111278.
[51] A. Rahmati, S.M. Varedi-Koulaei, M.H. Ahmadi, H. Ahmadi, Dimensional synthesis of the Stirling engine based on optimizing the output work by evolutionary algorithms, Energy Rep. 6 (2020) 1468–1486, https://doi.org/10.1016/j.egyr.2020.05.030.
[52] G.T. Udeh, S. Michailos, D. Ingham, K.J. Hughes, L. Ma, M. Pourkashanian, A new non-ideal second order thermal model with additional loss effects for simulating beta Stirling engines, Energy Convers. Manag. 206 (2020), 112493, https://doi.org/10.1016/j.enconman.2020.112493.
[53] F. Aksoy, H. Solmaz, H. Karabulut, C. Cinar, Y.O. Ozgoren, S. Polat, A thermodynamic approach to compare the performance of rhombic-drive and crank-drive mechanisms for a beta-type Stirling engine, Appl. Therm. Eng. 93 (2016) 359–367, https://doi.org/10.1016/j.applthermaleng.2015.09.105.
[54] C. Cinar, O. Ozdemir, H. Karabulut, M. Düzgün, Nodal Thermodynamic and Dynamic Analysis of a Free Displacer Stirling Engine, Isı Bilim. Ve Tek. Derg. (2021) 141–155, https://doi.org/10.47480/isibted.979390.
[55] H. Karabulut, F. Aksoy, E. Öztürk, Thermodynamic analysis of a β type Stirling engine with a displacer driving mechanism by means of a lever, Renew. Energy 34 (2009), https://doi.org/10.1016/j.renene.2008.03.011.
[56] H. Karabulut, H.S. Yücesu, C. Çinar, F. Aksoy, An experimental study on the development of a β-type Stirling engine for low and moderate temperature heat sources, Appl. Energy 86 (2009) 68–73, https://doi.org/10.1016/j.apenergy.2008.04.003.
[57] E.S. Aziz, C. Chassapis, Enhanced Hypocycloid Gear Mechanism for Internal Combustion Engine Applications, J. Mech. Des. Trans. ASME 138 (2016) 1–9, https://doi.org/10.1115/1.4034348.
[58] X. Xu, H. Xu, H. Deng, F. Gu, C. Talbot, An investigation of a hypocycloid mechanism based twin-rotor piston engine, Proc. Inst. Mech. Eng. Part C J. Mech. Eng. Sci. 229 (2015) 106–115, https://doi.org/10.1177/0954406214532632.
[59] F. Ahmed, S. Zhu, G. Yu, E. Luo, A potent numerical model coupled with multi-objective NSGA-II algorithm for the optimal design of Stirling engine, Energy 247 (2022), 123468, https://doi.org/10.1016/j.energy.2022.123468.
[60] Y. Hong, C.W. Lee, Pareto fronts for multiobjective optimal design of the lithium-ion battery cell, J. Energy Storage. 17 (2018) 507–514, https://doi.org/10.1016/j.est.2018.04.003.
[61] H.J. Lee, J.K. Shim, Multi-objective optimization of a dual mass flywheel with centrifugal pendulum vibration absorbers in a single-shaft parallel hybrid electric vehicle powertrain for torsional vibration reduction, Mech. Syst. Sig. Process. 163 (2022), 108152, https://doi.org/10.1016/j.ymssp.2021.108152.
[62] M. Unal, G.P. Warn, T.W. Simpson, Quantifying the shape of pareto fronts during multi-objective trade space exploration, J. Mech. Des. Trans. ASME 140 (2018), https://doi.org/10.1115/1.4038005.
[63] H. Li, B. Xu, G. Lu, C. Du, N. Huang, Multi-objective optimization of PEM fuel cell by coupled significant variables recognition, surrogate models and a multi-objective genetic algorithm, Energy Convers. Manag. 236 (2021), https://doi.org/10.1016/j.enconman.2021.114063.
[64] K. Deb, R. Datta, Hybrid evolutionary multi-objective optimization and analysis of machining operations, Eng. Optim. 44 (2012) 685–706, https://doi.org/10.1080/0305215X.2011.604316.